University of Dundee

Isolation and characterization of the gene HvFAR1 encoding acyl-CoA reductase from the cer-za.227 mutant of barley (Hordeum vulgare) and analysis of the cuticular barrier functions

Müller, Yannic; Patwari, Payal; Stöcker, Tyll; Zeisler-Diehl, Viktoria; Steiner, Ulrike; Campoli, Chiara

[Link to publication in Discovery Research Portal](#)

Isolation and characterization of the gene *HvFAR1* encoding acyl-CoA reductase from the *cer-za.227* mutant of barley (*Hordeum vulgare*) and analysis of the cuticular barrier functions

Yannic Müller[1]* (iD), Payal Patwari[1]* (iD), Tyll Stöcker[2] (iD), Viktoria Zeisler-Diehl[3] (iD), Ulrike Steiner[2], Chiara Campoli[4,5] (iD), Lea Grewe[1] (iD), Magdalena Kuczkowska[1], Maya Marita Dierig[1], Sarah Jose[6] (iD), Alistair M. Hetherington[6] (iD), Ivan F. Acosta[7] (iD), Heiko Schoof[2] (iD), Lukas Schreiber[3] (iD) and Peter Dörmann[1] (iD)

[1]Institute of Molecular Physiology and Biotechnology of Plants, University of Bonn, 53115 Bonn, Germany; [2]Institute of Crop Science and Resource Conservation, University of Bonn, 53115 Bonn, Germany; [3]Institute for Cellular and Molecular Botany, University of Bonn, 53115 Bonn, Germany; [4]Division of Plant Sciences, School of Life Sciences, University of Dundee, Dundee, DD2 5DA, UK; [5]James Hutton Institute, Dundee, DD2 5DA, UK; [6]School of Biological Sciences, University of Bristol, Bristol, BS8 1TQ, UK; [7]Max-Planck Institute for Plant Breeding Research, 50829 Cologne, Germany

Summary

• The cuticle is a protective layer covering aerial plant organs. We studied the function of waxes for the establishment of the cuticular barrier in barley (*Hordeum vulgare*). The barley *eceriferum* mutants *cer-za.227* and *cer-ye.267* display reduced wax loads, but the genes affected, and the consequences of the wax changes for the barrier function remained unknown.
• Cuticular waxes and permeabilities were measured in *cer-za.227* and *cer-ye.267*. The mutant loci were isolated by bulked segregant RNA sequencing. New *cer-za* alleles were generated by genome editing. The CER-ZA protein was characterized after expression in yeast and Arabidopsis *cer4-3*.
• *Cer-za.227* carries a mutation in *HORVU5Hr1G089230* encoding acyl-CoA reductase (FAR1). The *cer-ye.267* mutation is located to *HORVU4Hr1G063420* encoding β-ketoacyl-CoA synthase (KAS1) and is allelic to *cer-zh.54*. The amounts of intracuticular waxes were strongly decreased in *cer-ye.267*. The cuticular water loss and permeability of *cer-za.227* were similar to wild-type (WT), but were increased in *cer-ye.267*. Removal of epicuticular waxes revealed that intracuticular, but not epicuticular waxes are required to regulate cuticular transpiration.
• The differential decrease in intracuticular waxes between *cer-za.227* and *cer-ye.267*, and the removal of epicuticular waxes indicate that the cuticular barrier function mostly depends on the presence of intracuticular waxes.

Introduction

The cuticle forms the apoplastic barrier between aerial plant organs and the environment (Nawrath, 2006). It represents the first boundary of the plant and enhances the resistance against water loss, UV light, and pathogen attack and establishes a self-cleaning surface (Koch *et al.*, 2008; Lee & Suh, 2015). The protective capabilities of the cuticle depend on the presence of waxes which are embedded in (intracuticular) or overlaid onto (epicuticular) the cutin matrix forming crystalline structures on the surface (Nawrath, 2006; Koch *et al.*, 2008). Cuticular waxes are a mixture of very-long-chain fatty acid (VLCFA)-derivatives obtained from plastidial fatty acid *de novo* biosynthesis, often containing triterpenoids or sterols (Bernard & Joubès, 2013; Batsale *et al.*, 2021). Acyl-CoAs are transported to the endoplasmic reticulum (ER), where they are elongated by the fatty acid elongation (FAE) complex to give rise to VLCFA-CoAs. The FAE complex consists of four enzymes, β-ketoacyl-CoA synthase (KCS), β-ketoacyl-CoA reductase, β-hydroxyacyl-CoA dehydratase, and enoyl-CoA reductase. Different KCS subunits determine the chain length specificity of the FAE complexes (Millar & Kunst, 1997). VLCFA-CoAs are hydrolyzed by thioesterases to release free fatty acids, or they are reduced to aldehydes and decarbonylated to yield odd chain length alkanes, secondary alcohols, and ketones. In a third pathway, VLCFA is reduced to even chain length primary alcohols, which involves the formation of an aldehyde intermediate. Finally, waxes are exported from the plasma membrane, through the cell wall, and incorporated into the cuticle (Kunst & Samuels, 2009).

The identification of wax (*eceriferum*, *cer*) mutants was instrumental for the elucidation of the wax biosynthetic pathway. In *Arabidopsis thaliana*, 21 *cer* mutants were isolated with altered

wax loads or compositions on the stems (Koornneef *et al.*, 1989). Nevertheless, knowledge about the function of the individual wax components and fractions is still incomplete. The accumulation of cuticular waxes under drought for UV irradiation is a common adaptive mechanism for plants (Long *et al.*, 2003; Patwari *et al.*, 2019); therefore, identifying cuticular wax-related genes in crops broadens the scope for breeding strategies to enhance resilience against water loss during drought and heat stress (Mansour *et al.*, 2018). Barley (*Hordeum vulgare*) is the fourth most cultivated cereal world-wide (www.statistica.com), and an excellent genetic model thanks to the availability of genetic resources, including cultivars, landraces, wild relatives, and mutants (Mascher *et al.*, 2017). Numerous mutants have been isolated, mostly through UV, radioactive, or chemical mutagenesis (Lundqvist & Lundqvist, 1988; Lundqvist, 2014). A total of 1580 *cer* mutants of barley were isolated and assigned to 79 loci (Lundqvist & Lundqvist, 1988). The *cer-za* mutation with 78 alleles represents the fourth largest group behind *cer-c*, *cer-q*, and *cer-u* (Lundqvist & Lundqvist, 1988). Less frequent mutations are *cer-zh* (11 alleles) and *cer-ye* (5 alleles). Few *cer* genes in barley have been identified. The *cer-c*, *cer-q*, and *cer-u* loci are a cluster of genes on chromosome 2HS, coding for, respectively, a β-diketone synthase, a lipid/carboxyl transferase, and a P450 protein, and are crucial for the biosynthesis of β-diketones, the major component of the wax bloom on barley spikes and leaf sheaths (Schneider *et al.*, 2016). *CER-ZH* was identified as *HvKCS1*, required for fatty acid elongation (Li *et al.*, 2018). Recently, the HvSHINE1 transcription factor involved in the regulation of wax biosynthesis was found to be encoded by *CER-X* (McAllister *et al.*, 2022), while *CER-G* and *CER-S* were characterized as encoding two additional transcription factors, *HvYDA1* and *HvBRX-Solo*, regulating both cuticular integrity and cell patterning (Liu *et al.*, 2022).

To study the relevance of waxes as a cuticular barrier, we selected two *cer* mutants with a strong reduction in total leaf wax load, *cer-za.227* and *cer-ye.267* (Larsson & Svenningsson, 1986; Rostás *et al.*, 2008). Bulked segregant RNA sequencing (BSR-Seq) approaches revealed that *cer-za.227* contains a mutation in an acyl-CoA reductase (*HvFAR1*), while *cer-ye.267* is allelic *to cer-zh.54* which is mutated in *HvKCS1*. The analysis of different fractions of cuticular waxes revealed that *cer-ye.267*, but not *cer-za.227*, shows a significantly increased cuticular permeability, which can be attributed to alterations in the amounts of intracuticular waxes.

Materials and Methods

Plant material and cultivation conditions

Barley (*Hordeum vulgare* L.) seeds were obtained from the Nord-Gen seed bank (www.nordgen.org; Alnarp, Sweden; Supporting Information Table S1). The *cer-za.227* mutant was isolated after mutagenesis of the cultivar Foma (Lundqvist & Lundqvist, 1988; Bregitzer *et al.*, 2013). Gene isolation by mapping in the original mutant is hampered by the presence of background mutations. This issue was addressed by the generation of near-isogenic lines

(NILs) via repeated backcrossing of the original mutants to the cultivar Bowman (Druka *et al.*, 2011). A seven-times backcrossed *cer-za.227* line (BW157) was obtained from the Bowman NIL collection. Three further alleles in their original backgrounds, *cer-za.232* (Foma), *cer-za.318* (Foma), and *cer-za.173* (Bonus), were obtained (Bregitzer *et al.*, 2013; Table S1). For the *cer-ye.267* mutant (originally in cultivar Foma), we used the *cer-ye.267* NIL (BW136) which had been backcrossed to Bowman seven times (Druka *et al.*, 2011). Three allelic lines in the original backgrounds, *cer-ye.582* (Foma), *cer-ye.792* (Bonus), and *cer-ye.1395* (Bonus), were obtained (Table S1). Barley transformation was carried on in the early flowering line Golden Promise (GP-fast, Ppd-H1; Gol *et al.*, 2021).

The seeds were germinated on moistened filter paper in darkness for 3 d, after which the seedlings were transferred to pots with soil (Einheitserde ED73; Patzer, Sinntal-Altengronau, Germany) and vermiculite (3 : 1). The recessive mutants *cer-ye.267* (BW136) and *cer-zh.54* (Bonus) were crossed according to published protocols (Harwood, 2019).

Seeds of the *Arabidopsis thaliana* (L. Heynh.) *cer4-3* mutant were obtained from Gillian Dean (University of Vancouver, Canada; Rowland *et al.*, 2006). *Arabidopsis* seeds were surface-sterilized with chlorine gas and cultivated on Murashige and Skoog medium with 1% agarose and 1% sucrose for 2 wk before transfer to soil. *Nicotiana benthamiana* (Domin) seeds were directly sown into soil. All plants were cultivated in growth chambers at 21°C with 55% relative humidity and 16 h of light (150 μmol m^{-2} s^{-1}).

Cuticular wax analysis

Waxes were analyzed as described previously (Haas & Rentschler, 1984; Zeisler & Schreiber, 2016). Briefly, waxes were extracted from the second leaf of 14-d-old barley plants which were cut at 2 cm from the point of emergence (Richardson *et al.*, 2007), or from stems of 4-wk-old *Arabidopsis* plants. The plant organs were dipped into chloroform for 10 s, and the internal standard was added (10 μg tetracosane). The waxes were silylated and measured using gas chromatography (GC; Zeisler & Schreiber, 2016). For the selective removal of the epicuticular waxes, barley leaf sections 2 cm in length were treated with collodion (Haas & Rentschler, 1984). The epicuticular waxes were extracted from the strips, and the remaining (intracuticular) waxes were extracted from the stripped leaf. In addition, wax esters were measured by highly sensitive mass spectrometry (MS; Patwari *et al.*, 2019). Briefly, total waxes in chloroform were supplemented with internal standard (18:0ol-17:0), purified using a solid phase extraction and measured by direct infusion MS/MS (Patwari *et al.*, 2019).

Analysis of cuticular permeability and foliar water loss

The entire length of the second leaf of three-leaf stage barley plants was pressure sprayed for 3 s with a solution of 50 μM Metribuzin in 0.1% Brij-L4 (Merck, Darmstadt, Germany). The quantum yield of chlorophyll fluorescence of photosystem II

(quantum yield of PSII), a measure for the penetration of the photosynthetic inhibitor into the leaf, was monitored with a pulse-amplitude modulation fluorometer (Walz, Effeltrich, Germany). Leaves were dark-adapted, and the quantum yield of PSII was measured during the treatment in 5-min intervals for 3 h by applying PSII-saturating light flashes.

Foliar water loss was determined as published (Grünhofer *et al.*, 2022). Total water permeance of the leaf (predominantly representing transpiration through the stomata) was measured with an SC-1 Leaf Porometer (Decagon Devices Inc., Pulman, WA, USA). Residual water permeance (representing transpiration through the cuticle) of the detached leaves was gravimetrically measured in constant intervals throughout an incubation at 2% humidity and 25°C. The leaves were finally dried to determine their dry weights.

Determination of contact angles and scanning electron microscopy

Leaf-water drop contact angles were determined with a Drop Shape Analyzer (DSA25; KRÜSS, Hamburg, Germany). For imaging epicuticular wax crystals, leaf sections of 14-d-old barley plants were mounted on carbon-coated aluminum stubs and dried in a desiccator. The dry samples were sputter-coated with gold (5 nm; Automatic Sputter Coater; Ingenieurbüro Peter Liebscher, Wetzlar, Germany). Images were acquired using a scanning electron microscope (Phenom-World, Eindhoven, the Netherlands; or TESCAN GmbH, Dortmund, Germany).

Mutagenesis of the *CER-ZA* locus

Two 20-bp sequences containing protospacer adjacent motifs (PAMs) on exons 5 and 8 of *CER-ZA* were targeted by the design of two single-guide RNAs (sgRNA1, 5′-GGAAACCCCTCG AAAACAGA; sgRNA2, 5′-GAACTTGCAGAGGCTAAGAG) using CAS-DESIGNER (Park *et al.*, 2015). The sgRNA sequences were assembled from two oligonucleotides each (sgRNA1, bn4388, bn4389; sgRNA2, bn4390, bn4391; Table S2) and cloned into pMG625 and pMG627 and then introduced into pMP217 via Golden Gate cloning using *Bsa*I/*Bbs*I. The recipient plasmid pMP217 (derivative of pMGE599) harbors hygromycin B and Cas9 endonuclease genes, both driven by the maize ubiquitin promoter. The construct pMP217-sgRNA1-sgRNA2 was transferred into barley embryos (Golden Promise) as recently described (Amanda *et al.*, 2022). Transgenic calli were selected on hygromycin B and the plantlets transferred into soil. The two PAM sites were screened for mutations by a PCR amplification of their genomic DNA (sgRNA1, bn4748, bn4749; sgRNA2, bn4752, bn4753; Table S2). The PCR products were ligated into pJET1.2 (Thermo Fisher Scientific, Dreieich, Germany). Eight *E. coli* clones per PAM site and per plant were sequenced.

Semiquantitative RT-PCR and subcellular localization

A strip of leaf epidermis was carefully removed from 10-d-old Bowman seedlings using forceps (Weyers & Travis, 1981). Total RNA was isolated from the epidermal strip, the stripped leaf, and the roots (NucleoSpin RNA Plant; Macherey-Nagel, Düren, Germany) and used for cDNA synthesis (RevertAid First Strand cDNA Synthesis Kit; Thermo Fisher Scientific). RT-PCR was performed for *CER-ZA* (*HORVU5Hr1G089230*, bn4254, bn4255), *CER-YE* (*HORVU4Hr1G063420*, bn4275, bn4276) and the housekeeping gene *ACT2* (*AY145451.1*, bn3698, bn3699). Primers were designed using Primer3 (Table S2; Untergasser *et al.*, 2012).

The coding sequence of CER-ZA was PCR-amplified from the cDNA of Bowman leaves (bn4045, bn4046; Table S2) and ligated into the *Bam*HI/*Sal*I sites of pLH9000-GFP-WSD1 carrying the *35S* promoter (Patwari *et al.*, 2019). The pLH9000-GFP-CER-ZA construct, the ER marker (pCB-DsRed-HDEL; Patwari *et al.*, 2019), and pMP19 (Voinnet *et al.*, 2000) were transferred into *Agrobacterium* GV3101. The *Agrobacterium* cells were infiltrated into the abaxial side of *N. benthamiana* leaves and observed with a spinning disc confocal microscope (IX73; Olympus Optical, Tokyo, Japan; DSU filter turret Lambda 10-3, Sutter Instrument, Novato, CA, USA; Linear laser system 400 Series, Oxford Instruments, Oxford, UK). DsRed fluorescence was excited at 561 nm, and its emission was observed with a center wavelength of 607.36 nm. GFP fluorescence was excited at 488 nm, and its emission was filtered with a center wavelength of 525.3 nm. A depth of 290 nm was covered in 30 planes.

Expression of CER-ZA in *Saccharomyces cerevisiae* and *Arabidopsis*

The coding sequence of CER-ZA was PCR-amplified from Bowman cDNA (bn4277, bn4171, Table S2). The amplicon was ligated into pJet1.2, released with *Eco*RI/*Sal*I, and ligated into the yeast vector pDR196 (Rentsch *et al.*, 1995). The pDR196-CER-ZA construct was introduced into *Saccharomyces cerevisiae* BY4741 (Euroscarf, Oberursel, Germany). After growth at 28°C for 72 h, the cells were harvested by centrifugation (3500 g, 10 min). Lipids were extracted with chloroform/methanol (2 : 1) in the presence of the internal standard (1-heptadecanol, 5 μg). The organic phase was harvested after centrifugation, the solvent was evaporated, and the fatty acids were transmethylated with 1 M methanolic HCl (80°C, 1 h). Lipids were extracted with hexane/0.9% NaCl (1 : 1) and separated by thin-layer chromatography in hexane/diethyl ether/acetic acid (55 : 45 : 0.5) on silica plates. After staining with 8-anilinonaphthalene-1-sulfonic acid, the free alcohols were isolated from the silica with hexane/0.9% NaCl (1 : 1). After centrifugation, the organic phase was collected and the solvent evaporated. Alcohols were dissolved in chloroform and silylated with pyridine and N,O-bis-(trimethylsilyl)-trifluoroacetamide (BSTFA; 30 min, 70°C). The silylated alcohols were analyzed using gas chromatography–mass spectrometry (GC–MS) (helium flow, 1.05 ml min^{-1}; split/splitless injection; inlet temperature, 250°C; septum flow, 3 ml min^{-1}; initial oven temperature, 120°C for 2 min, ramped at 10°C min^{-1} to 180°C, held for 2 min, increased to 310°C, held for 10 min, decrease of 5°C min^{-1} to 120°C).

The promoter and terminator regions of *CER4* were PCR-amplified from *Arabidopsis* Col-0 genomic DNA (Rowland *et al.*, 2006). The *CER-ZA* sequence was amplified from Bowman leaf cDNA (bn3955, bn3956, Table S2). The binary vector pBin-35S-eGFP-DsRed (Patwari *et al.*, 2019) was digested with *SmaI/MluI* to remove the entire eGFP cassette and ligated with the three *BsaI*-digested fragments (*CER4* promoter, *CER-ZA* cDNA, *CER4* terminator) using Golden Gate cloning. The construct pBIN-AtCER4pro::CER-ZA-AtCER4term-DsRed was transferred into *Agrobacterium* GV3101 and transferred into the *Arabidopsis cer4-3* mutant (Zhang *et al.*, 2006). Four independent homozygous transgenic lines were selected in the T_3 generation based on red seed fluorescence.

Results

Alterations in water repellence and surface structure in *cer-za.227* and *cer-ye.267*

After spraying with water, water droplets were not retained on the leaf surfaces of wild-type (WT) barley cultivar Bowman, but accumulated on *cer-za.227* and *cer-ye.267* (Fig. 1a). The contact angles of the water droplets on WT Bowman leaves are very large due to the high hydrophobicity of the wax layer, with values > 150°. The contact angles of water droplets on *cer-za.227* (122.2 ± 2.6°) and *cer-ye.267* (119.9 ± 7.4°) were decreased, indicating that the wettability of the mutant leaves was increased.

Scanning electron microscopy revealed that Bowman leaves are densely covered with platelet-shaped wax crystals. The number of crystals was reduced, and the crystals were unevenly distributed on the surfaces of *cer-za.227* and *cer-ye.267* (Fig. 1b). The morphology of the crystals of *cer-za.227* was altered, with fewer platelet-shaped structures accompanying an increase in tubular forms. The structure of wax crystals in *cer-ye.267* was not altered, although the density of wax crystals appeared lower (Fig. 1). Because *cer-za.227* and *cer-ye.267* had similar wax amounts

(Fig. 2a), the auto-assembly of waxes into crystals might be affected.

Changes in wax load and composition in *cer-za.227* and *cer-ye.267*

The total wax load and composition were determined in the leaves of Bowman and the *cer-za.227* (BW157) and *cer-ye.267* (BW136) mutants (Fig. 2a). The epicuticular (surface) and the intracuticular (embedded into the cutin matrix) waxes were separately extracted and measured. In Bowman, the total wax load was 11.5 µg cm^{-2}, 4/5 of which were epicuticular waxes. Total waxes declined to 3.2 µg cm^{-2} in *cer-za.227* (28%, all percentages compared with Bowman), and 3.4 µg cm^{-2} in *cer-ye.267* (30%). In *cer-za.227*, the epicuticular waxes were particularly decreased (1.8 µg cm^{-2}, 19%), while the intracuticular waxes were less affected (1.4 µg cm^{-2}, 60%) (Fig. 2a). In *cer-ye.267*, the epicuticular waxes were less affected (2.3, 26%), and the intracuticular waxes were strongly decreased (1.1 µg cm^{-2}, 46%). The decrease in intracuticular waxes was more pronounced in *cer-ye.267* compared with *cer-za.227* (Fig. 2a).

Most wax classes were decreased in the two mutants (Fig. 2b). The cuticular waxes of barley leaves are dominated by primary alcohols, mostly 1-hexacosanol (26:0ol) (Nødskov Giese, 1975). Alcohols (26:0ol) were strongly reduced in *cer-za.227* and *cer-ye.267* (Fig. S1). The alkane content (mostly C33) was increased in *cer-za.227*, but it was decreased in *cer-ye.267*. The contents of aldehydes, particularly 26:0al and 28:0al, and esters (C40, C42, C44, and C46) were reduced in *cer-za.227* and *cer-ye.267*, except the C40 ester which was increased in *cer-ye.267* (Fig. S1). Highly sensitive wax ester measurements by direct infusion MS/MS analysis confirmed that the amounts of wax esters were decreased in *cer-za.227*, particularly those containing 26:0ol (Fig. S2). The total wax loads were also decreased by 50–70% in the three alleles of *cer-za* (*cer-za.173*, *cer-za.232*, and *cer-za.318*) and *cer-ye* (*cer-ye.582*, *cer-*
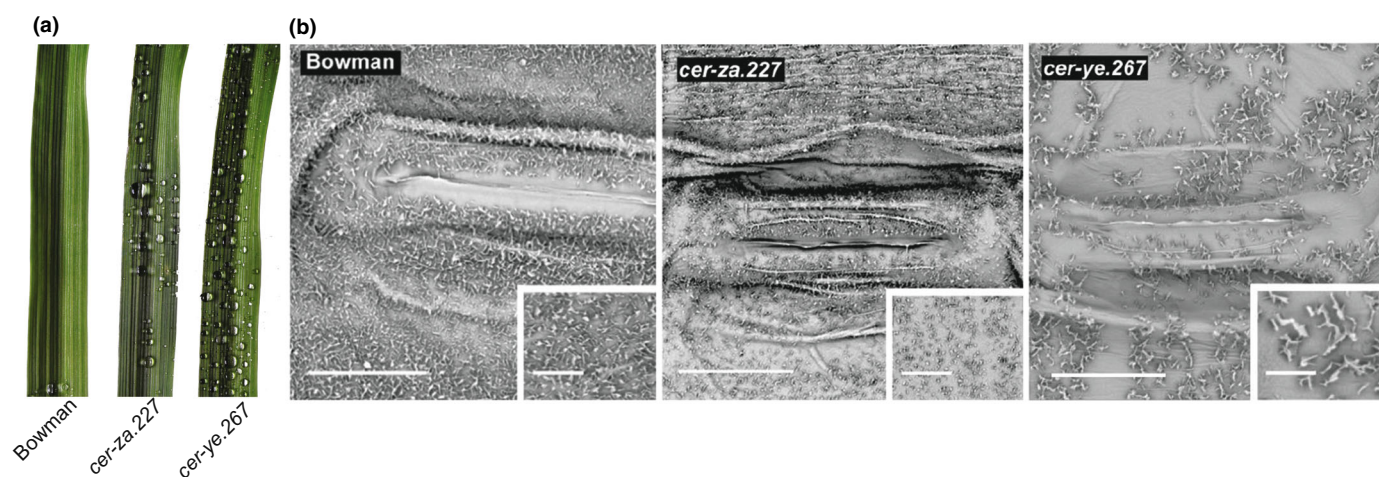
Fig. 1 Wettability and surface structures of barley cultivars Bowman, *cer-za.227* and *cer-ye.267*. (a) Water droplets accumulate on the surfaces of *cer-za.227* and *cer-ye.267* leaves but roll off the leaf surface of the Bowman cultivar. (b) Scanning electron microscopy of leaf surfaces reveals a dense coverage with plate-shaped crystalline waxes on Bowman leaves, but a low number of wax crystals on *cer-za.227* and *cer-ye.267* leaves. Bars: (b) 10 µm; (insets) 8 µm.
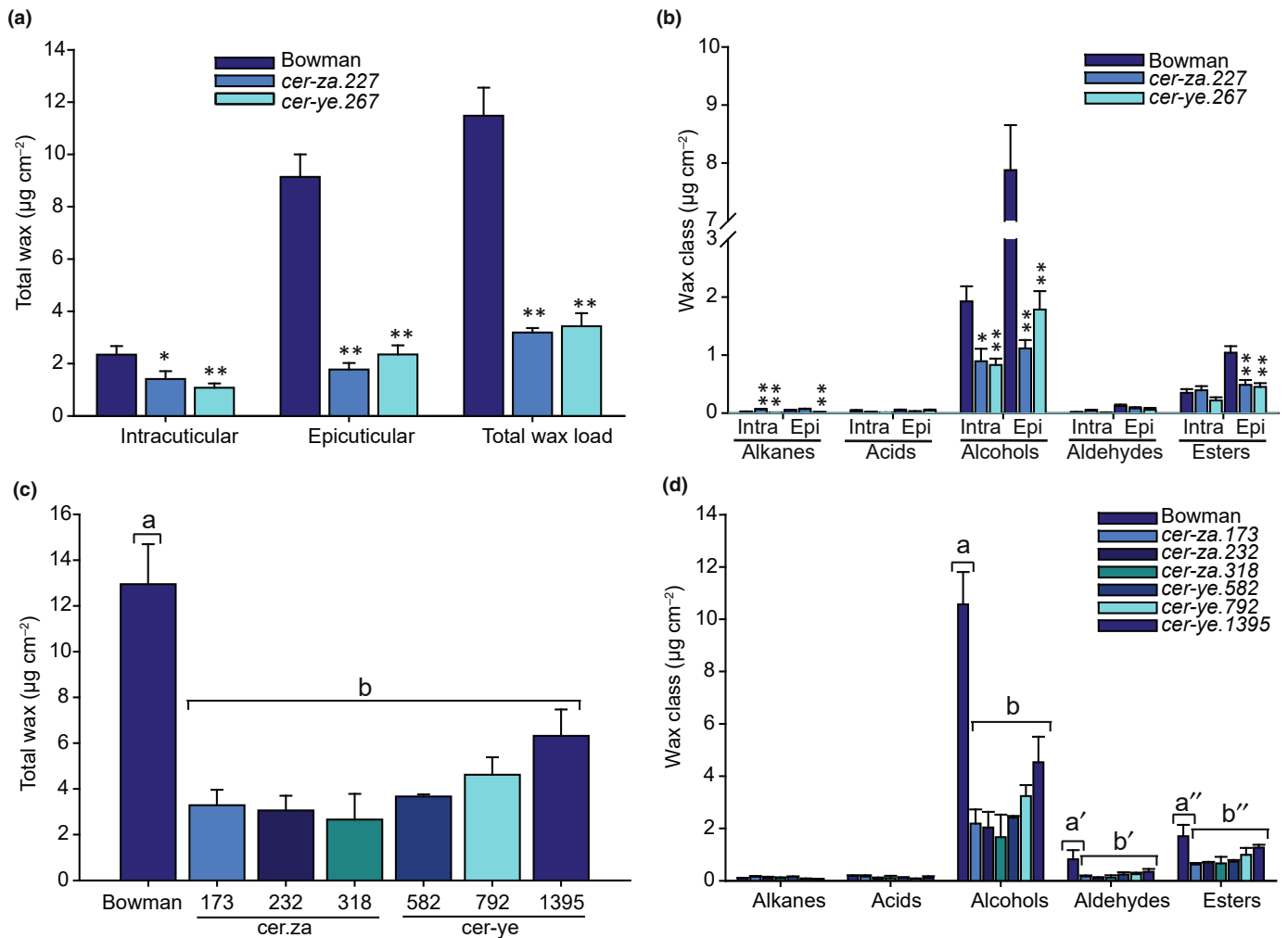
Fig. 2 Cuticular wax load and composition of *cer-za* and *cer-ye* mutant alleles. Waxes were extracted from the leaves, and the wax components were quantified using gas chromatography (GC-FID). (a) Total waxes of the epicuticular (isolated) and intracuticular (remaining) wax fractions, extracted from the leaves of barley cultivars Bowman, *cer-za.227*, and *cer-ye.267*. (b) Different wax classes in the epicuticular and intracuticular wax fractions. (d) Wax classes from different *cer-za* and *cer-ye* alleles. (c) Total cuticular waxes from *cer-za* and *cer-ye* alleles. The wax loads and composition of the cultivar Bowman were very similar to those of Foma (*cer-za.232*, *cer-za.318*, *cer-ye.267*, and *cer-ye.582*) and Bonus (*cer-za.173*, *cer-ye.792*, and *cer-ye.1395*). Mean ± SD; $n = 3$; (a, b): *t*-test, significant differences to Bowman are indicated (**, $P < 0.01$; *, $P < 0.05$) (c, d) ANOVA, different letters indicate significant differences with $P < 0.05$. In (d), a, b, a′, b′ and a″, b″ refer to the comparison of the amounts of alcohols, aldehydes and esters from the different lines, respectively.

ye.792, and *cer-ye.1395*) compared with Bowman (Fig. S1). The total wax load and composition of the different cultivars (Bowman, Bonus, Foma, and Golden Promise) were highly similar. The changes in the wax load and composition of the three additional *cer-za* and *cer-ye* alleles tested were very similar to *cer-za.227 and cer-ye.267*, respectively (Fig. 2c,d).

The *cer-za.227* mutation is located to *HORVU5Hr1G089230*

BSR-Seq represents a powerful method to identify mutant genes in small populations (Dong *et al.*, 2018; Wu *et al.*, 2018). The *CER-ZA* locus was mapped in a F₂ population from a cross of *cer-za.227* with Bowman (Methods S1). Using BSR-Seq, we identified an elevated mutant allele SNP frequency in the region of 580–660 Mb on chromosome 5, in agreement with previous

results (Druka *et al.*, 2011; Bregitzer *et al.*, 2013). This region (Fig. S3) carries 49 genes with high-confidence SNPs compared with the Morex sequence (Mascher *et al.*, 2017). The number of candidate genes was narrowed down by comparing their expression levels between the Bowman control and the *cer-za.227* bulks, removing genes with similarly abundant RNA reads (Table S3). The analysis of the remainder of the genes for their predicted functions allowed us to identify *HORVU5Hr1G089230* as a candidate for CER-ZA. Computation of the Δ(SNP-index; Takagi *et al.*, 2013) and the *G′* values (Magwene *et al.*, 2011) of the most likely causal SNPs positioned *HORVU5Hr1G089230* among the three most likely genes for CER-ZA. Furthermore, the transcript abundance of *HORVU5Hr1G089230* was clearly downregulated in the *cer-za.227* bulk compared with Bowman (log₂ fold change: −2.2; false discovery rate (FDR) 1.704×10^{-20}).

HORVU5Hr1G089230 encodes a protein of 498 amino acids with a calculated mass of 55.95 kDa. According to AHRD prediction, it encodes a FAR likely involved in wax biosynthesis. 'NAD_binding_4' and 'sterile' domains were predicted by Pfam, and a Rossmann fold within the NAD_binding_4 domain (amino acids 11–57) with NADP as potential cofactor was identified using Cofactory. The sterile domain (also known as FAR_C) is shared by members of the FAR family. A transmembrane domain was predicted at the C terminus by TMHMM, in accordance with DeepLoc, which indicated that *HORVU5Hr1G089230* is membrane-bound and ER-localized. Therefore, *CER-ZA* is likely *HORVU5Hr1G089230*, which is predicted to encode a membrane-bound, ER-localized protein with FAR activity. Protein BLAST searches in barley revealed that HORVU5Hr1G089230 belongs to a family of 22 FAR proteins (Table S4). Sequences of FAR proteins from different plants were used to construct a phylogenetic tree (Fig. S4). HORVU5Hr1G089230 clusters with FAR1 from the grasses *Aegilops* and *Brachypodium*. The FAR sequences form four clades with a split of predicted ER-localized FARs from monocots (clade I) or dicots (clade II), and a separation of plastid-localized FARs into clades III (dicots) and IV (monocots), the latter in agreement with previous results (Zhang *et al.*, 2021).

The BSR-Seq approach revealed 10 SNPs in *HORVU5Hr1G089230* of *cer-za.227* compared with Morex_V2 (Fig. 3a; Table S5). Because the sequence around the *cer-za.227* mutation is presumably derived from Foma, most of the SNPs (1–4 and 6–10) are due to polymorphisms between Foma and Morex. Only SNP5 was specific for *cer-za.227*. SNP5 caused a guanine deletion at position 584526708 of chromosome 5, associated with a frameshift in exon 4 which causes the exchange of Asn153Ile, a premature stop codon, and the truncation of the polypeptide after 153 amino acids (Fig. 3a,b). Comparison of the RNA-Seq sequence of the other alleles with their respective WT cultivars revealed the presence of further SNPs. The *cer-za.318* allele displayed the same mutation as *cer-za.227*; therefore, these two SNPs might be derived from the same mutagenesis event. The *cer-za.232* mutant carried a thymine/adenine exchange at position 584526341 at the exon5/intron5 splicing site after Lys229, leading to the translation of the intron sequence and a premature stop codon after 253 amino acids. Finally, *cer-za.173* contains a cytosine/adenine exchange at position 584525054, resulting in a Glu331 stop mutation in exon 8. The amino acid sequences of HORVU5Hr1G089230 in Bonus and Morex are identical, while the Foma sequence differs by two amino acids (Asn34Asp and Ala627Tyr). The protein structures (modeled with Alphafold) revealed the presence of a Rossmann fold and are highly similar for all cultivars (www.uniprot.org) (Fig. 3b). The HORVU5Hr1G089230 polypeptides of *cer-za.227* and *cer-za.318* are truncated, lacking a large part of the C terminus. Similarly, the protein sequences of *cer-za.232* and *cer-za.173* are truncated, and the structures are strongly affected (Fig. 3c).

Generation of *cer-za* alleles by genome editing

To prove that *HORVU5Hr1G089230* is *CER-ZA*, we mutagenized *HORVU5Hr1G089230* by genome editing. Barley Golden Promise was transformed with constructs harboring the Cas9 endonuclease and two sgRNA sequences targeted to PAM sites in exons 5 and 8. Two independent lines, *cer-za.2001* and *cer-za.2002*, were regenerated. Sequencing of the regions around the PAM site in exon 5 revealed that *cer-za.2001* is heteroallelic, with a thymine insertion in one and a thymine deletion in the other allele, while *cer-za.2002* is homoallelic, with thymine deletions (Fig. 4a). After spraying with water, water droplets rolled off the leaves of Golden Promise, but they adhered to the leaves of the *cer-za* mutants obtained by genome editing, similar to *cer-za.227* (Fig. 4a). The total wax load was decreased from 16.3 µg cm^{-2} in Golden Promise to 5.7 µg cm^{-2} in *cer-za.2001* and 6.7 µg cm^{-2} in *cer-za.2002*, and this was mainly based on the decrease in 26:0ol (Fig. 4a). Therefore, *cer-za.2001* and *cer-za.2002* display changes in wettability, wax load, and composition analogous to *cer-za.227*, demonstrating that *HORVU5Hr1G089230* is *cer-za.227*.

Expression of CER-ZA in yeast and *Arabidopsis cer4-3*

CER-ZA was expressed in *Saccharomyces cerevisiae* to study its enzymatic function. After expression, lipids were extracted from the cells and analyzed using GC–MS. The *CER-ZA*-expressing cells accumulated primary alcohols, hexadecanol (16:0ol), octadecanol (18:0ol), and hexacosanol (26:0ol) (Fig. 4b). CER-ZA is therefore capable of producing primary alcohols, in particular 26:0ol, indicating that it harbors alcohol-forming FAR activity.

The *AtFAR3/CER4* gene product from *Arabidopsis* produces 24:0ol and 26:0ol alcohols (Rowland *et al.*, 2006). As a consequence, waxes on the stems of the *cer4* mutant are deficient in primary alcohols. To study the *in planta* function, *CER-ZA* was introduced into the *Arabidopsis cer4-3* mutant under control of the *AtCER4* promoter to confer its epidermal expression. Four independent homozygous *CER-ZA*-expressing *cer4-3* plants were selected, and the wax load and composition on the stems were measured (Fig. 4c). The wax ester content was increased in all *CER-ZA-cer4-3* lines compared with *cer4-3*, albeit without reaching WT levels. Concomitantly, the primary alcohol content was doubled in *CER-ZA-cer4-3* lines compared with *cer4-3*, but it also did not reach WT levels. The amounts of alkanes and aldehydes in the transgenic lines were slightly increased compared with WT and *cer4-3*, while the secondary alcohol contents were unchanged. The expression of *CER-ZA* in *cer4-3* therefore results in the accumulation of primary alcohols, indicating that it harbors FAR activity *in planta*.

The *cer-ye.267* mutation localizes to *HORVU4Hr1G063420* and is allelic to *cer-zh.54*

The computation of the Δ(SNP-index) (Takagi *et al.*, 2013) and the *G'* values (Magwene *et al.*, 2011) for the SNPs between the Bowman and *cer-ye.267* bulks led to the identification of regions on chromosomes 2H, 4H, and 5H with *G'* values above the threshold (FDR = 0.01; Fig. S5). We focused on chromosome 4 where this mutation was previously reported to be located (Druka *et al.*, 2011). The region of 490–530 Mbp contains seven genes
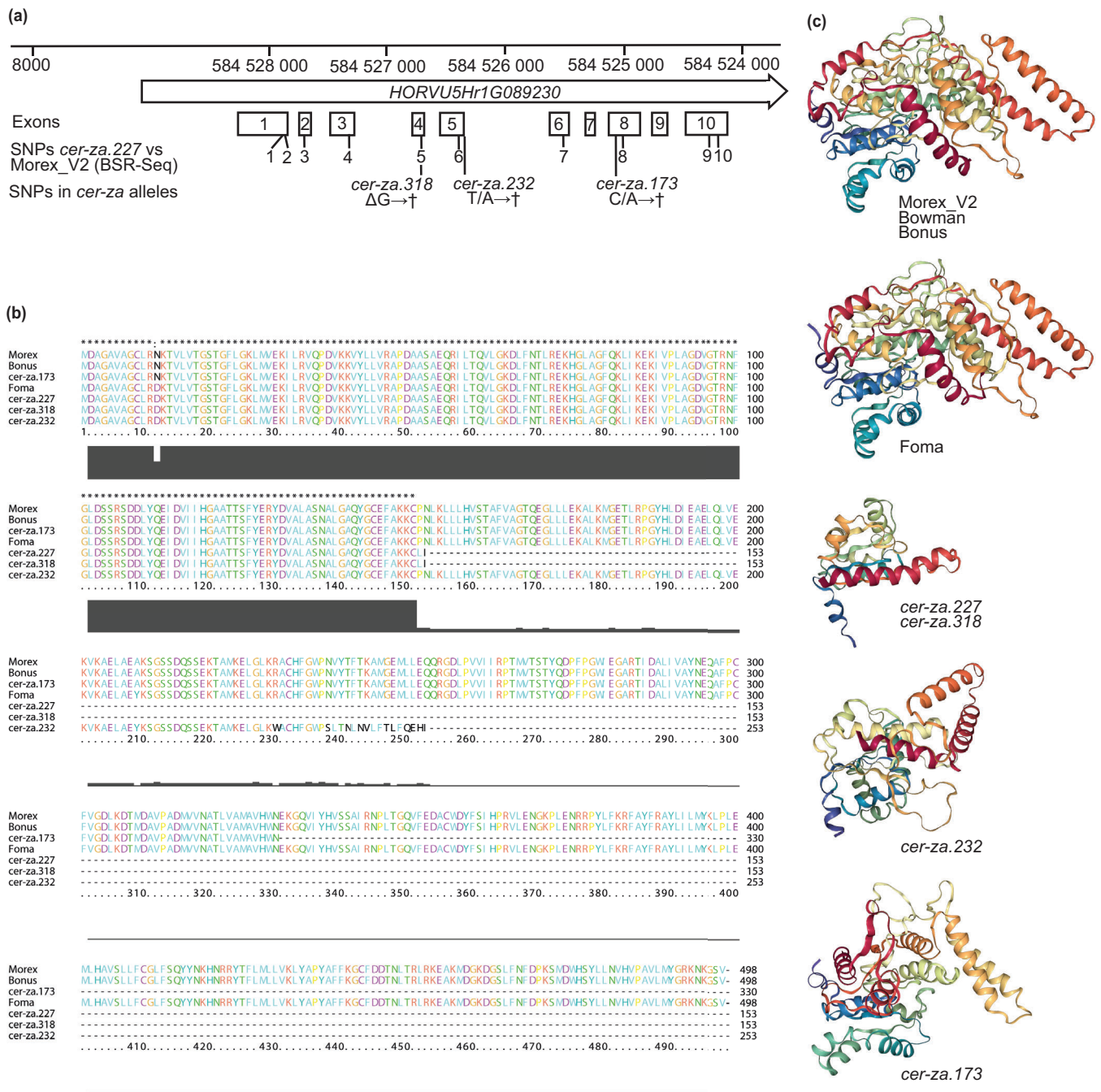
Fig. 3 *cer-za* mutations are associated with SNPs in the gene *HORVU5Hr1G089230*. (a) Representation of the *HORVU5Hr1G089230* locus. The diagram shows its position on chromosome 5H, the exon/intron structure, the SNPs between *cer-za.232* and the reference sequence of Morex_V2, the SNPs between *cer-za.173* and Bonus, and the SNPs between *cer-za.232* and *cer-za.318* and Foma. The deletion of G (ΔG) in *cer-za.227* and *cer-za.318* in exon 8 results in a premature stop codon (†). The T-to-A exchange at the splicing site after exon 5 in *cer-za.232*, and the C-to-A exchange in exon 8 of *cer-za.173*, also cause the introduction of premature stop codons. (b) Protein sequences based on SNPs identified busing BSR-Seq for the different *cer-za* alleles in comparison with Morex, Foma, and Bonus. The amino acid sequences of Morex, Bowman, and Bonus are identical. Foma differs from this sequence by two amino acids. Bars indicate the degree of identity between all sequences at a given position. (c) Protein models calculated by Alphafold. Proteins of *cer-za.227*, *cer-za.318*, *cer-za.232*, and *cer-za.173* are truncated, lacking considerable parts of the C-terminal structural elements.

with high-confidence SNPs (Table S6). Combining this approach with the screening for differentially induced genes indicated that *HORVU4Hr1G063420* is a likely candidate for *cer-ye.267*. This gene covers 2979 bp with an intron-less coding sequence of 1638 bp, encoding a protein of 545 amino acids.

The *cer-ye.267* sequence harbors a thymine/adenine exchange compared with Morex_V2 and Foma at position 1940 (Fig. 5a), which results in a Phe495Tyr exchange. RNA-Seq analysis of the additional *cer-ye* alleles revealed that *cer-ye.792* and *cer-ye.1395* carry an identical SNP of cytosine/adenine at position 1068
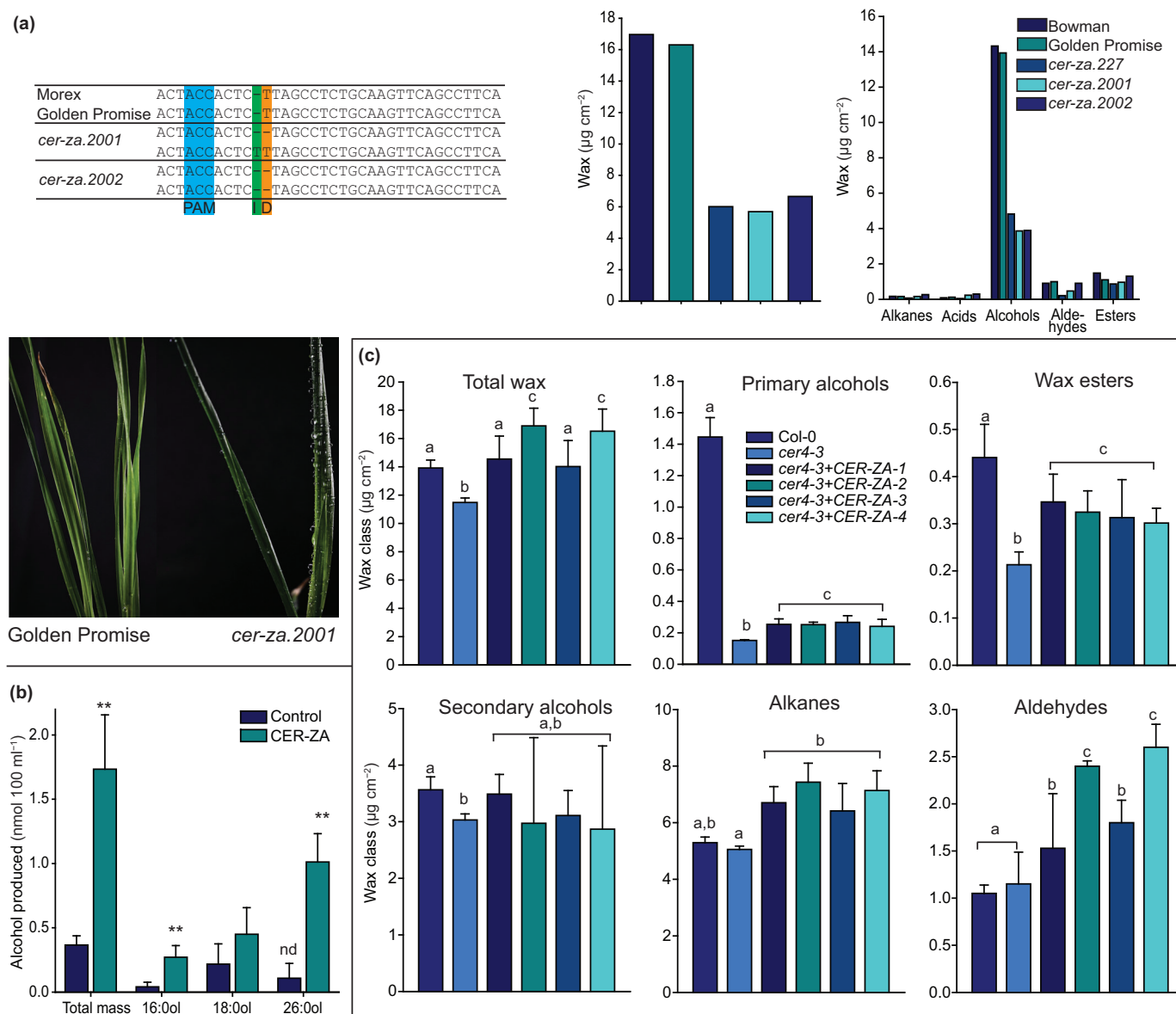
Fig. 4 *CER-ZA* gene product harbors acyl-CoA reductase activity. (a) The *eceriferum* mutant plants *cer-za.2001* and *cer-za.2002* generated by genome editing. Alignment of the DNA sequences around the protospacer adjacent motif (PAM, blue) in exon 5 of *HORVU5Hr1G089230*. Sequences of barley cultivars Morex, Golden Promise, and the alleles of the two mutant lines. The sequence of *cer-za.2001* shows an insertion (I, green) of a T in one allele and a deletion (D, orange) of a T the other one. The sequence of *cer-za.2002* is homoallelic with a deletion of a T. The water droplets adhere to the leaves of the *cer-za* alleles obtained by genome editing (shown here: *cer-za.2001*), in contrast to Golden Promise. Total amount and composition of cuticular waxes on the leaves of *cer-za.227*, *cer-za.2001*, and *cer-za.2002*. Only single measurements of waxes of the genome-edited lines *cer-za.2001* and *cer-za.2002* were possible due to the limitation of leaf material. (b) The *CER-ZA* sequence was expressed in *Saccharomyces cerevisiae*. Lipids were isolated from cells obtained from 100 ml ($OD_{600} = 1$) and, after conversion into trimethylsilyl ethers, measured using gas chromatography–mass spectrometry (GC–MS) with total ion chromatograms (TIC). Three primary alcohols accumulated in *CER-ZA* -expressing cells: 16:0ol, 18:0ol, and a very-long-chain alcohol identified as 26:0ol. 26:0ol showed the strongest increase. Note that the peak eluting at the retention time of 26:0ol is a contaminant with a different mass spectrum (nd, not detected). Mean ± SD; $n = 3$; t-test; significant differences to the control (empty vector); **, $P \leq 0.01$. (c) Wax analysis of the stems of four independent *Arabidopsis thaliana cer4-3* mutant plants expressing *CER-ZA* from barley. Cuticular waxes were isolated from the stems of transformed *cer4-3* plants and measured using GC–MS. The panels show total wax coverage and the distribution of wax classes. Mean ± SD; $n = 3$; ANOVA; different letters indicate significant differences; $P < 0.05$.

compared with both Morex and Bonus, causing a premature stop codon, and a truncated protein (Fig. 5b). No SNP was found in the *HORVU4Hr1G063420* sequence of *cer-ye.582* compared with Morex or Bonus. Fig. 2 shows that *cer-ye.582* has the same wax phenotype as *cer-ye.267*; therefore, *cer-ye.267* might carry a

mutation in the regulatory sequences (promoter or intron), but these sequences were not covered within the RNA-Seq approach.

HORVU4Hr1G063420 was previously identified as the gene underlying the *cer-zh.54* mutation (Li *et al.*, 2018). *CER-ZH* encodes HvKCS1, and consequently, the *cer-zh.54* mutant is wax

deficient and shows the typical adhesion of water droplets on the leaf. To confirm allelism, *cer-ye.267* and *cer-zh.54* were crossed, and F$_1$ plants were analyzed after spraying the leaves with water. A dense accumulation of water droplets was observed on the leaves of the F$_1$ plants, demonstrating that *cer-ye.267* and *cer-zh.54* are allelic (Fig. 5c).

Expression of CER-ZA and CER-YE and the subcellular localization of CER-ZA

CER-ZA/HvFAR1 and *CER-YE/HvKCS1* are likely expressed in the leaf epidermis, in analogy with numerous genes involved in wax biosynthesis (Suh *et al.*, 2005). The expression was studied using semiquantitative RT-PCR after the isolation of an epidermal strip from the leaves of Bowman, compared with the residual stripped leaf and the roots. Bands of 196 and 238 bp corresponding to *CER-ZA* and *CER-YE*, respectively, were observed in the epidermal tissue after electrophoresis, but were absent from the roots or residual leaf material (Fig. 6a). This is consistent with RNA-Seq data (EoRNA database; Milne *et al.*, 2021). *CER-ZA/ HvFAR1* (locus BART1_0-p38542) displays low transcript abundance in the roots, apical meristems, spikes, anthers/microspores grains/seeds (including embryo, lemma, palea, lodicule, and rachis), moderate expression in the leaves, and coleoptiles, and high expression in the epidermis. Similarly, *CER-YE/HvKCS1* (BART1_0-p30122) is highly expressed in the leaves and epidermis and shows considerable expression in the root maturation zones, lemma, palea and stat-like/multicellular microspores, and low expression in the roots and seeds. Therefore, *CER-ZA* and *CER-YE* are highly expressed in the leaf epidermis, while *CER-YE* is expressed in additional tissues.

CER-ZA was predicted to be ER-localized using DeepLoc. In addition, CER-ZA carries a C-terminal KNKGSV sequence related to the prototypic dilysine ER-retrieval motif KXKXX, also found in the ER-resident fatty acid desaturase FAD3 of *Arabidopsis* (McCartney *et al.*, 2004). To study its subcellular localization experimentally, the CER-ZA sequence was fused to the C terminus of the green fluorescent protein (GFP) and transiently expressed in *N. benthamiana* leaves. A DsRed-HDEL construct was co-infiltrated as a marker for the ER. The GFP and DsRed fluorescence were observed using confocal fluorescence microscopy. After co-infiltration, the two signals were observed in a net-like structure in epidermal cells (Fig. 6b). The merged signals revealed a clear overlap, confirming that CER-ZA localizes to the ER.

Mutation of *cer-ye.267*, but not *cer-za.227*, affects the function of the cuticular barrier

To study the consequences of the wax changes for the barrier function, the permeation properties of the cuticles of *cer-za.227* and *cer-ye.267* were measured after treatment with the photosynthetic inhibitor Metribuzin (Fig. 7a). The quantum yield of PSII was used as a measure for the penetration rate of Metribuzin across the cuticular barrier. After the application of Metribuzin to the leaves, the quantum yield of PSII decreased within 25 min from 0.7 to *c.* 0.48 in Bowman and *cer-za.227*, indicating that the

penetration rates were similar. The quantum yield of PSII drastically declined in *cer-ye.267* reaching values as low as *c.* 0.25, then it slowly recovered to *c.* 0.4, but was always lower than in Bowman and *cer-za.227*. Therefore, Metribuzin penetrated the cuticle of *cer-ye.267* much faster than that of Bowman or *cer-za.227*.

Water loss through the epidermis can be explained by transpiration through stomata and by water evaporation through the cuticle. Under normal conditions with open stomata, transpiration through the stomata is predominant. Therefore, the total water permeance of a leaf is mostly caused by transpiration through the stomata. The total water permeance was determined by measuring the water flow for the adaxial and abaxial leaf sites with a porometer. The total water permeance did not differ between Bowman, *cer-za.227*, and *cer-ye.267*, indicating that transpiration through the stomata was not affected (Fig. 7b). This was in agreement with the finding that stomatal sizes and densities were very similar to Bowman as revealed by microscopic inspection of the leaf surfaces. Next, the water permeance of detached leaves was measured and plotted against the relative water deficit (RWD; Fig. S6). The water permeance was initially high for all lines, but then rapidly declined due to stomatal closure to reach final values of residual permeance P_{min}, which were *c.* 95% lower. The P_{min}, which is a proxy for the cuticular transpiration rate, was calculated from the averages of the measurements after stomatal closure in the range of RWD of 0.15–0.55 (Figs 7c, S6). The P_{min} of *cer-za.227* (2.14 ± 0.56 nm s^{-1}) was slightly but not significantly higher compared with Bowman (1.63 ± 0.18 nm s^{-1}; 95% significance level, *t*-test, $P = 0.086$), whereas P_{min} of *cer-ye.267* (2.35 ± 0.35 nm s^{-1}; $P = 0.0005$) was even higher and significantly increased compared with Bowman. Therefore, the penetration rate of Metribuzin and the cuticular transpiration are not significantly changed in *cer-za.227*, but both are compromised in *cer-ye.267*.

To study the roles of intracuticular and epicuticular waxes for water permeability directly, the water loss of a barley leaf was recorded starting 1 h after detachment. At this time, the stomata were closed, and the residual water loss is a measure of cuticular transpiration. After one additional h, the epicuticular waxes were removed with collodion, and the measurements were continued. The rate of water loss did not change after removal of the epicuticular waxes (Fig. 7d). Therefore, cuticular transpiration rates do not depend on the presence of epicuticular waxes. Fig. 7(e) shows an electron micrograph of the leaf surface with the removal of epicuticular waxes on the left side, leaving behind the layer of intracuticular waxes, while the right side remained untreated. This experiment demonstrates that intracuticular waxes rather than epicuticular waxes are crucial for the cuticular barrier function of barley.

Discussion

The cuticle establishes a barrier between the plant and the environment, providing essential protection against abiotic and biotic stresses. The composition of the cuticular wax layer has been studied in detail, but the contribution of the different wax fractions to the barrier functions remains unclear. The two barley mutants
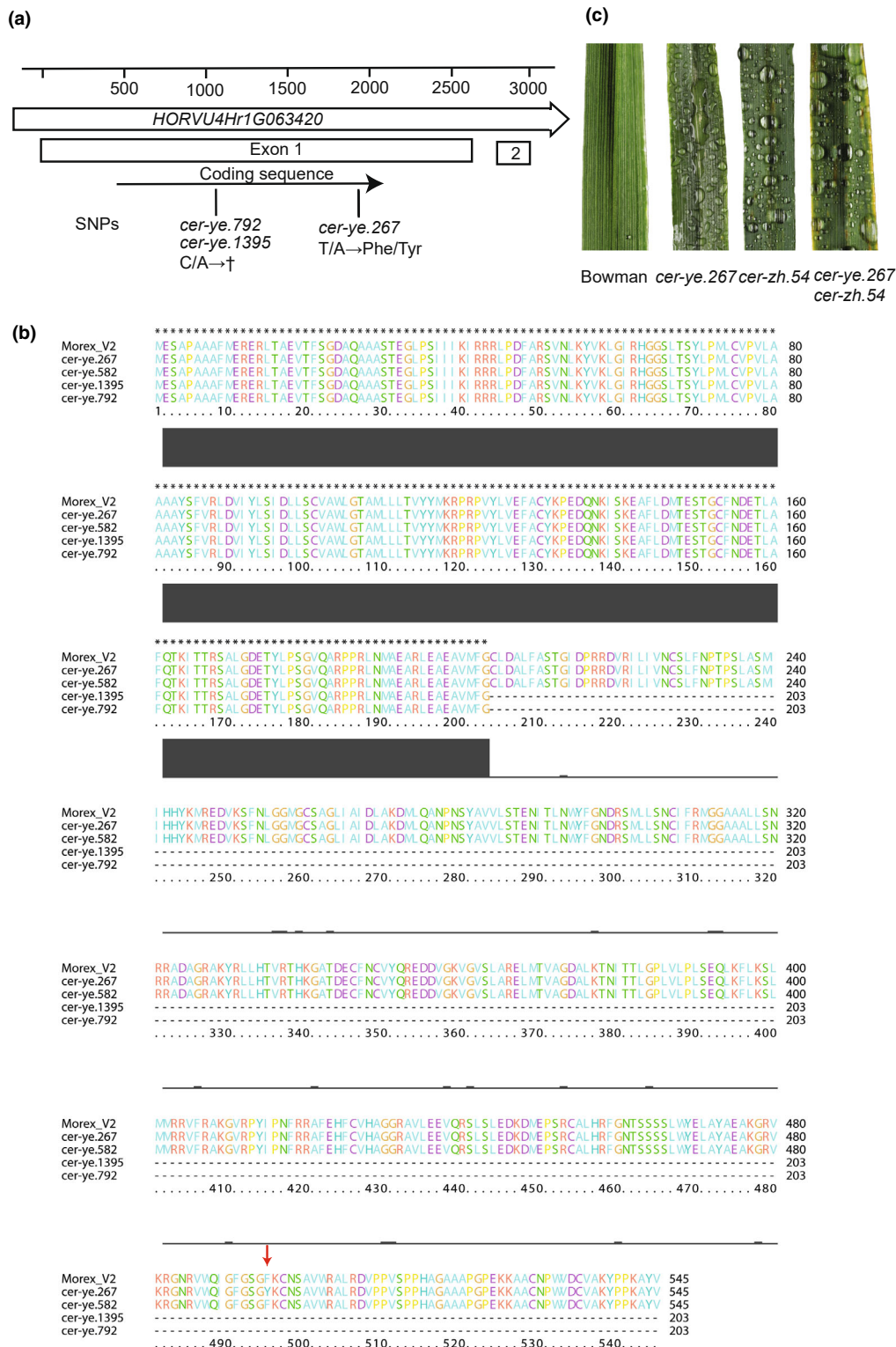
Fig. 5 *cer-ye* mutations are caused by SNPs in the gene *HORVU4Hr1G063420*. (a) Representation of the *HORVU4Hr1G063420* locus. The diagram shows the position on chromosome 4H, the exon/intron structure, and the SNPs between *cer-ye.267*, *cer-ye.792*, and *cer-za.1395* and the reference sequence of Morex_V2. The *cer-ye.267* mutation of T/A causes an amino acid exchange of Phe/Tyr. The *cer-ye.792* and *cer-ye.1395* mutants carry the same mutation of C/A resulting in a premature stop codon (†). (b) Protein sequences based on SNPs identified using BSR-Seq for Morex and the different *cer-za* alleles, *cer-ye.267*, *cer-ye.582*, *cer-ye.1395*, and *cer-ye.792*. The amino acid sequences of barley cultivars Morex, Bowman, and Bonus are identical. Bars indicate the degree of identity between all sequences. The position of the amino acid exchange Phe/Typr in *cer-ye.267* is depicted with a red arrow. (c) Allelism test for *cer-ye.267* (BW136) and *cer-zh.54* (Bonus). The two mutants *cer-ye.267* and *cer-zh.54* were crossed, and leaves from the plants of the F₁ generation were sprayed with water to determine the wettability of the leaf surface. No water droplets adhere to leaves of Bowman (shown as control) or Bonus.
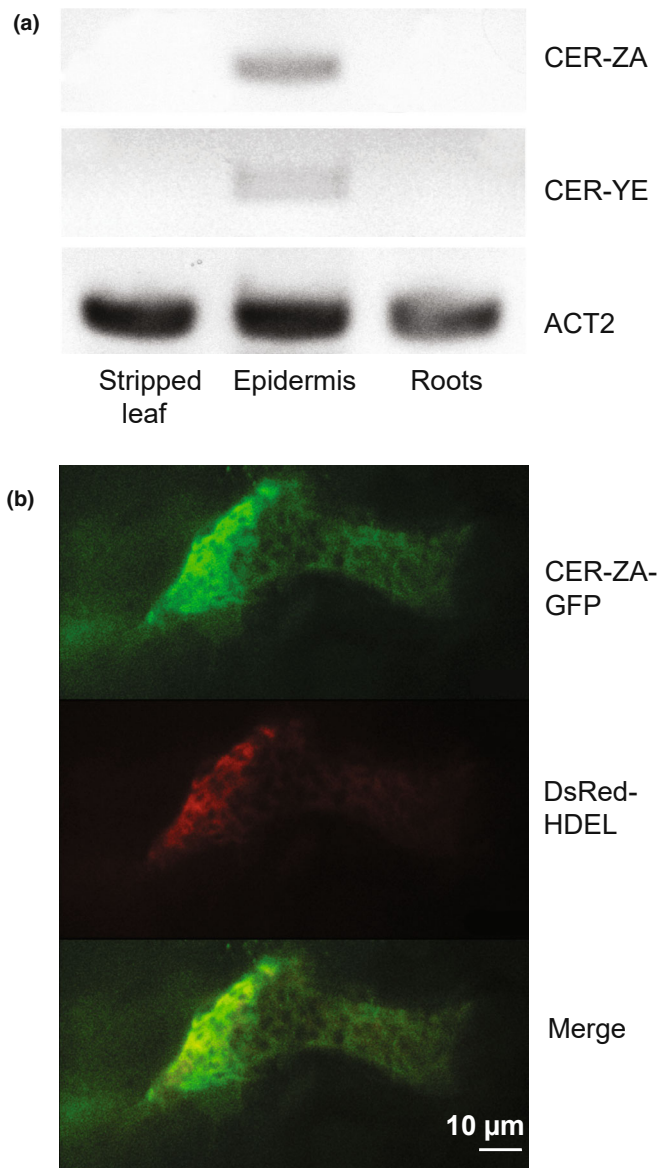
Fig. 6 Expression analysis of barley cultivars *CER-ZA* and *CER-YE* and subcellular localization of CER-ZA. (a) Expression of CER-ZA and CER-YE was compared using a semiquantitative RT-PCR of RNA isolated from epidermal strips of leaves, the stripped leaf, and the root tissue. The *ACT2* gene was used as the control. RT-PCR bands were separated using agarose gel electrophoresis and stained with Midori green. (b) Subcellular localization of CER-ZA. The CER-ZA sequence was fused to the C terminus of GFP, and the GFP-CER-ZA construct expressed in *Nicotiana benthamiana* leaves together with the endplasmic reticulum (ER) marker DsRed-HDEL. Epidermal leaf cells were observed using confocal fluorescence microscopy.

cer-za.227 and *cer-ye.267* reveal strong decreases in total wax load, but unique changes in wax composition and the epicuticular and intracuticular distribution. The *CER-ZA* gene was identified as *HORVU5Hr1G089230*, encoding HvFAR1, while the mutation in *cer-ye.267* is allelic to *cer-zh.54*, which corresponds to *HORVU4Hr1G063420*, encoding HvKCS1. In contrast to *cer-za.227*, the *cer-ye.267* mutation affected the barrier functions, which are therefore presumably established by unique properties in wax distribution rather than a decrease in total wax load.

Identification of the *CER-ZA* and *CER-YE* genes

The gene *HORVU5Hr1G089230* was identified as CER-ZA by BSR-Seq and confirmed by the generation of novel *cer-za* alleles. *CER-ZA* represents the first *FAR* characterized in barley. A total of 22 and eight FAR sequences were annotated in barley and Arabidopsis, respectively (Table S4; Aarts *et al.*, 1997; Doan *et al.*, 2009, 2012). FAR enzymes were characterized in wheat and *Brachypodium* (Wang *et al.*, 2015b, 2018; Chai *et al.*, 2018). Expression in yeast confirmed that CER-ZA harbors alcohol-forming FAR activity similar to AtFAR3/CER4 (Rowland *et al.*, 2006). CER-ZA localizes to the ER, in analogy with the FARs in *Arabidopsis* (Rowland *et al.*, 2006) and wheat (Wang *et al.*, 2015b; Chai *et al.*, 2018). Some *FARs*, including *AtFAR1*, *AtFAR4*, and *AtFAR5*, are expressed in the leaves and roots and therefore also contribute to suberin biosynthesis (Domergue *et al.*, 2010). *CER-ZA* is highly expressed in the leaf epidermis, but not in the roots (Fig. 6a), similar to *AtFAR3/CER4*, suggesting that the two proteins are functional orthologs. The expression of *CER-ZA* in the *Arabidopsis cer4-3* mutant led to increases in the amounts of primary alcohols and wax esters, however without reaching WT levels; therefore, *CER-ZA* partially restores the wax deficiency of *cer4-3*, similar to *TaFAR2*, *TaFAR3*, *TaFAR3*, *TaFAR5*, *BdFAR1*, *BdFAR2*, and *BdFAR3* from wheat and *Brachypodium* (Wang *et al.*, 2015b, 2016, 2018). Possibly, the heterologous FARs from monocots localize to different subcompartments of the ER, resulting in an incomplete complementation of *cer4* (Wang *et al.*, 2015a).

The *cer-ye.267* mutation (BGS 448) was located in *HORVU4Hr1G063420* (Fig. S5). The same locus was previously linked to *cer-zh.54*, and the *cer-ye.267* and *cer-zh.54* mutations were confirmed to be allelic (Fig. 6c). CER-ZH (HvKCS1) is a member of a family of 33 KCS sequences in barley (Li *et al.*, 2018; Tong *et al.*, 2021), but only one other KCS (HvKCS6/EMR1) was functionally characterized (Weidenbach *et al.*, 2015). KCS enzymes are involved in fatty acid metabolism, cutin and suberin biosynthesis, and developmental processes (Lee *et al.*, 2009; Voisin *et al.*, 2009). Expression in yeast showed that CER-ZH elongates C16/C18 saturated and monounsaturated fatty acids up to C22 carbon atoms, which can presumably be elongated by other KCSs (Li *et al.*, 2018).

Wax composition of *cer-za.227* and *cer-ye.267*

The *cer-za.227* and *cer-ye.267* mutations decreased the total wax load by *c.* 70% (Fig. 2), in agreement with previous results using *cer-za.126* and *cer-zh.54* (Rostás *et al.*, 2008; Li *et al.*, 2018). The amounts of epicuticular waxes were strongly decreased. Intracuticular waxes were less affected in *cer-za.227*, and they were strongly decreased in *cer-ye.267* (Fig. 2). The most prominent change in the two mutants was the decline in the amount of 26:0ol. In *cer-za.227*, the amounts of aldehydes (26:0al) and wax esters were decreased, while alkanes (mostly C33) accumulated. Primary alcohols and wax esters are derived from the reductive pathway, whose initial step is catalyzed by FAR (Haslam *et al.*, 2017). A restriction in the production of primary alcohols

consequently affects substrate availability for wax ester biosynthesis. Alkane production is increased, possibly due to an increase in the carbon flux into the decarbonylation pathway, which gives rise to aldehyde and alkane production. The decrease in the amounts of aldehydes in *cer-za.227* might be explained by rapid decarbonylation of aldehydes to alkanes, or by a reduced production of aldehydes through the reductive pathway as a side product of FAR. The amounts of all wax classes, including alcohols,
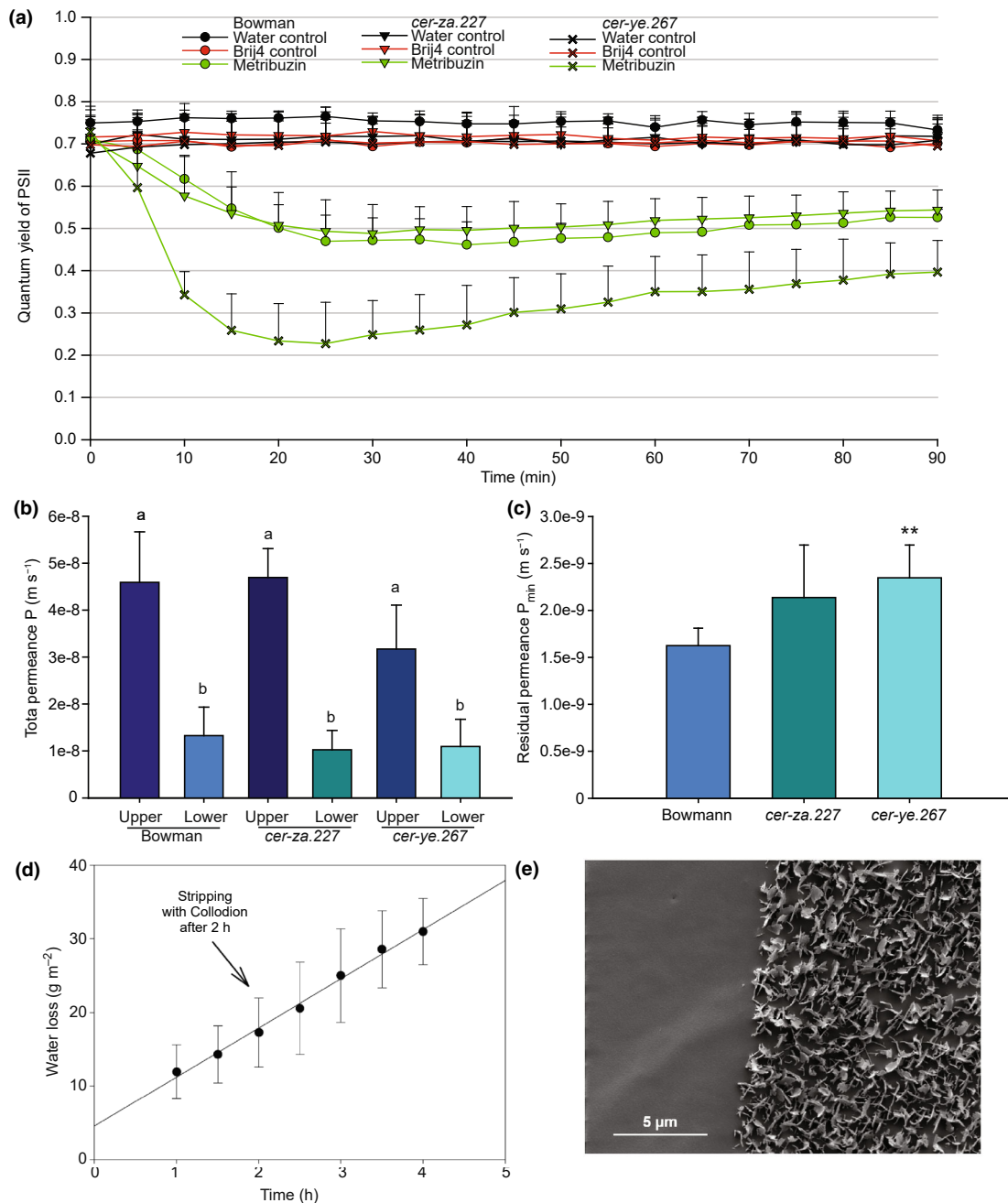

Fig. 7 Permeability and water loss through the cuticle of the leaves of the barley *cer-za.227* and *cer-ye.267* mutants. (a) The quantum yield of Photosystem II (PSII) was recorded as a measure of the penetration of the photosynthetic inhibitor Metribuzin across the cuticular barrier of Bowman, *cer-za.227*, and *cer-za.267*. Brij 4 and water controls were added to exclude effects by components of the spray solution. Mean ± SD; $n = 3$. (b) Stomatal transpiration rates given as total permeance P (m s^{-1}) of the adaxial and abaxial sites of five leaves each of Bowman, *cer-za.227* and *cer-za.267* determined using a leaf porometer. Means ± SD; $n = 5$; ANOVA; different letters indicate differences with $P < 0.05$. (c) Residual permeance P_{min} (transpiration through the cuticle). The P_{min} values were calculated from the means of individual measurements after stomatal closing, as shown in Supporting Information Fig. S6. Data show means and the 95% confidence intervals (CI) for Bowman ($n = 35$), *cer-za.227* ($n = 50$), and *cer-ye.267* ($n = 50$); t-test; **, $P < 0.01$. (d) Water loss of a leaf (cultivar Golden Promise) was recorded 1 h after detachment when stomata were closed, thus representing residual water permeance (cuticular transpiration). After one additional h, the epicuticular waxes were stripped off with collodion, and the measurements continued. Mean ± SD, $n = 3$. (e) Scanning electron micrograph of the leaf surface (Golden Promise). Epicuticular waxes have been stripped with collodium on the left side of the leaf, leaving behind the intracuticular waxes, while the right side, which was not treated, displays the coverage with epicticular waxes.

aldehydes, esters, alkanes and acids, were decreased in cer-ye.267, in analogy with *cer-zh.54* (Larsson & Svenningsson, 1986; Li *et al.*, 2018). The *cer-ye.267* and *cer-zh.54* lines carry mutations in HvKCS1, involved in acyl chain elongation. The two mutants displayed changes in chain length distribution of wax esters, because long-chain esters were decreased compared with short ones (Fig. S1j; Li *et al.*, 2018). It is possible that the HvKCS1 activity is redundant with other HvKCS proteins in barley (Li *et al.*, 2018). Furthermore, the amount of alkanes was decreased in *cer-ye.267* rather than increased as in *cer-za.267*. Although these two plants carry mutations in genes of wax biosynthetic enzymes, they result in a different distribution between intracuticular and epicuticular waxes. This might be caused by differences in the wax composition, which might alter their auto-assembly and affect the ratio of intracuticular to epicuticular waxes (Koch *et al.*, 2008).

Wax crystal formation and self-cleaning effect

Primary alcohols in the epicuticular waxes play an important role for the formation of plate-shaped crystals, which render the surface super-hydrophobic (Koch *et al.*, 2006). Bowman leaves are densely covered with plate-like crystals. The number of crystals was reduced in *cer-za.228* and *cer-ye.267*, which both displayed decreased amounts of 26:0ol, in agreement with previous results for *cer-za.126* and *cer-zh.54* (Rostás *et al.*, 2008; Li *et al.*, 2018). The crystals provide an efficient self-cleaning effect, resulting in decreased water droplet angles and compromised water repellence. Therefore, deficiency in epicuticular wax in *cer-za.227* and *cer-ye.267* affects their self-cleaning properties and water repellence.

Water loss and cuticular permeability in *cer-za.227* and *cer-ye.267*

The intracuticular waxes in *cer-za.227* are decreased to *c.* 60% of Bowman levels, and the remaining amount was still sufficient to establish a functional barrier for Metribuzin and to maintain a slightly but not significantly increased cuticular transpiration rate (Fig. 7). The amount of intracuticular waxes in *cer-ye.267* is decreased to *c.* 46% of Bowman levels, and the permeability for Metribuzin and the cuticular transpiration were significantly increased (Fig. 7). Direct measurements of residual water loss of a leaf after collodion treatment demonstrated that intracuticular rather than epicuticular waxes are relevant for establishing the cuticular transpiration barrier (Fig. 7d,e). These results are in good agreement with previous findings, which showed that cuticular barrier functions are primarily established by intracuticular waxes (Jetter & Riederer, 2016; Zeisler & Schreiber, 2016; Zeisler-Diehl *et al.*, 2018). No simple and linear relationship between cuticular barrier properties and wax amounts was found for different species (Riederer & Schreiber, 2001), or for the same species (Sadler *et al.*, 2016; Grünhofer *et al.*, 2022). The cuticular permeability remained unchanged or it increased in a set of seven cuticle mutants of Arabidopsis, with decreases or increases in wax or cutin amounts. Therefore, the coordinated

deposition and the semicrystalline arrangement of the highly ordered wax barrier within the cuticle might have been disturbed in the mutants with increased permeabilities. This could also be the reason for the altered cuticular permeability of *cer-ye.267* (Fig. 7). In contrast to the total wax load, alkanes and esters were proposed to contribute to the establishment of a functional transport barrier (Larsson & Svenningsson, 1986; W. Wang *et al.*, 2015; Bueno *et al.*, 2019; Li *et al.*, 2020; Wu *et al.*, 2022). The amount of alkanes was increased in *cer-za.227*, possibly contributing to the barrier function, but it was decreased in *cer-ye.267* (Fig. S2). Although the wax ester content was decreased, this effect was restricted to the epicuticular waxes. The *cer-ye.267* and *cer-zh.54* mutants showed a shift in chain length distribution of wax esters (Fig. S1j; Li *et al.*, 2018) possibly contributing to the modulation of cuticular permeability. Conversely, the strong reduction in the amounts of primary alcohols (26:0ol) did not affect the cuticular barrier function in *cer-za.227*, and it therefore cannot be the cause for increased permeability and cuticular transpiration in *cer-ye.267*. Instead, primary alcohols, which are abundant in Poaceae, presumably fulfill other functions in crystal formation and water repellence and light reflection (Fig. S2; Koch *et al.*, 2006).

In conclusion, the two barley lines *cer-za.227* and *cer-ye.267*, which carry mutations in two genes involved in wax biosynthesis, *HvFAR1* and *HvKCS1*, respectively, reveal a strong reduction in total wax amounts, distinct changes in composition, and amounts of intracuticular to epicuticular waxes. These changes caused an increase in cuticular permeability (Fig. 7a) in *cer-ye.267*, but not in *cer-za.227*. Therefore, the decrease in cuticular barrier function in *cer-ye.267* compared with *cer-za.227* is presumably explained by the differences in wax composition and a reduction in intracuticular waxes. The precise role of the individual wax lipids for the establishment of the (intra)cuticular barrier, however, remains to be discovered.

Competing interests

None declared.

Author contributions

YM, PP, US, HS, LS, and PD conceived and designed experiments. YM, PP, VZ-D, LG, MK, and MMD performed the experiments. YM, PP, TS, US, HS, LS, and PD analyzed the data. TS, US, CC, SJ, AMH, IA, HS, and LS contributed bioinformatic, genetic resources. YM, PP, TS, and PD wrote the manuscript with contributions from all authors. YM and PP contributed equally to this work.

ORCID

Ivan F. Acosta https://orcid.org/0000-0001-7080-3384
Chiara Campoli https://orcid.org/0000-0001-7809-2927
Peter Dörmann https://orcid.org/0000-0002-5845-9370
Lea Grewe https://orcid.org/0000-0001-7593-7840
Alistair M. Hetherington https://orcid.org/0000-0001-6060-9203
Sarah Jose https://orcid.org/0000-0003-2737-6473
Yannic Müller https://orcid.org/0000-0002-6974-4951
Payal Patwari https://orcid.org/0000-0003-1356-6639
Heiko Schoof https://orcid.org/0000-0002-1527-3752
Lukas Schreiber https://orcid.org/0000-0001-7003-9929
Tyll Stöcker https://orcid.org/0000-0001-7184-9472
Viktoria Zeisler-Diehl https://orcid.org/0000-0001-7050-9716

Data availability

Raw sequencing data (transcriptomic sequencing, RNA-Seq) have been deposited at the Sequence Read Archive (SRA) of the National Center for Biotechnology Information (NCBI) with accession no. PRJNA890449.

References

Aarts MG, Hodge R, Kalantidis K, Florack D, Wilson ZA, Mulligan BJ, Stiekema WJ, Scott R, Pereira A. 1997. The Arabidopsis MALE STERILITY 2 protein shares similarity with reductases in elongation/condensation complexes. *The Plant Journal* **12**: 615–623.

Amanda D, Frey FP, Neumann U, Przybyl M, Šimura J, Zhang Y, Chen Z, Gallavotti A, Fernie AR, Ljung K et al. 2022. Auxin boosts energy generation pathways to fuel pollen maturation in barley. *Current Biology* **32**: 1798–1811.

Batsale M, Bahammou D, Fouillen L, Mongrand S, Joubès J, Domergue F. 2021. Biosynthesis and functions of very-long-chain fatty acids in the responses of plants to abiotic and biotic stresses. *Cells* **10**: 1284.

Bernard A, Joubès J. 2013. Arabidopsis cuticular waxes: advances in synthesis, export and regulation. *Progress in Lipid Research* **52**: 110–129.

Bregitzer P, Lundqvist U, Carollo BV. 2013. Descriptions of barley genetic stocks for 2013. *Barley Genetics Newsletter* **43**: 48–223.

Bueno A, Alfarhan A, Arand K, Burghardt M, Deininger A-C, Hedrich R, Leide J, Seufert P, Staiger S, Riederer M. 2019. Effects of temperature on the cuticular transpiration barrier of two desert plants with water-spender and water-saver strategies. *Journal of Experimental Botany* **70**: 1613–1625.

Chai G, Li C, Xu F, Li Y, Shi X, Wang Y, Wang Z. 2018. Three endoplasmic reticulum-associated fatty acyl-coenzyme a reductases were involved in the production of primary alcohols in hexaploid wheat (*Triticum aestivum* L.). *BMC Plant Biology* **18**: 41.

Doan TTP, Carlsson AS, Hamberg M, Bülow L, Stymne S, Olsson P. 2009. Functional expression of five Arabidopsis fatty acyl-CoA reductase genes in *Escherichia coli. Journal of Plant Physiology* **166**: 787–796.

Doan TTP, Domergue F, Fournier AE, Vishwanath SJ, Rowland O, Moreau P, Wood CC, Carlsson AS, Hamberg M, Hofvander P. 2012. Biochemical characterization of a chloroplast localized fatty acid reductase from *Arabidopsis thaliana. Biochimica et Biophysica Acta (BBA) – Bioenergetics* **1821**: 1244–1255.

Domergue F, Vishwanath SJ, Joubès J, Ono J, Lee JA, Bourdon M, Alhattab R, Lowe C, Pascal S, Lessire R et al. 2010. Three Arabidopsis fatty acyl-coenzyme A reductases, FAR1, FAR4, and FAR5, generate primary fatty alcohols associated with suberin deposition. *Plant Physiology* **153**: 1539–1554.

Dong W, Wu D, Li G, Wu D, Wang Z. 2018. Next-generation sequencing from bulked segregant analysis identifies a dwarfism gene in watermelon. *Scientific Reports* **8**: 2908.

Druka A, Franckowiak J, Lundqvist U, Bonar N, Alexander J, Houston K, Radovic S, Shahinnia F, Vendramin V, Morgante M et al. 2011. Genetic dissection of barley morphology and development. *Plant Physiology* **155**: 617–627.

Gol L, Haraldsson EB, von Korff M. 2021. Ppd-H1 integrates drought stress signals to control spike development and flowering time in barley. *Journal of Experimental Botany* **72**: 122–136.

Grünhofer P, Herzig L, Sent S, Zeisler-Diehl VV, Schreiber L. 2022. Increased cuticular wax deposition does not change residual foliar transpiration. *Plant, Cell & Environment* **45**: 1157–1171.

Haas K, Rentschler I. 1984. Discrimination between epicuticular and intracuticular wax in blackberry leaves: ultrastructural and chemical evidence. *Plant Science Letters* **36**: 143–147.

Harwood WA. 2019. An introduction to barley: the crop and the model. *Methods in Molecular Biology* **1900**: 1–5.

Haslam TM, Gerelle WK, Graham SW, Kunst L. 2017. The unique role of the ECERIFERUM2-LIKE clade of the BAHD acyltransferase superfamily in cuticular wax metabolism. *Plants* **6**: 23.

Jetter R, Riederer M. 2016. Localization of the transpiration barrier in the epi- and intracuticular waxes of eight plant species: water transport resistances are associated with fatty acyl rather than alicyclic components. *Plant Physiology* **170**: 921–934.

Koch K, Barthlott W, Koch S, Hommes A, Wandelt K, Mamdouh W, De-Feyter S, Broekmann P. 2006. Structural analysis of wheat wax (*Triticum aestivum*, c.v. 'Naturastar' L.): from the molecular level to three dimensional crystals. *Planta* **223**: 258–270.

Koch K, Bhushan B, Barthlott W. 2008. Diversity of structure, morphology and wetting of plant surfaces. *Soft Matter* **4**: 1943.

Koornneef M, Hanhart CJ, Thiel F. 1989. A genetic and phenotypic description of *eceriferum* (*cer*) mutants in *Arabidopsis thaliana. Journal of Heredity* **80**: 118–122.

Kunst L, Samuels L. 2009. Plant cuticles shine. advances in wax biosynthesis and export. *Current Opinion in Plant Biology* **12**: 721–727.

Larsson S, Svenningsson M. 1986. Cuticular transpiration and epicuticular lipids of primary leaves of barley (*Hordeum vulgare*). *Physiologia Plantarum* **68**: 13–19.

Lee S-B, Jung S-J, Go Y-S, Kim H-U, Kim J-K, Cho H-J, Park OK, Suh M-C. 2009. Two Arabidopsis 3-ketoacyl CoA synthase genes, KCS20 and KCS2/DAISY, are functionally redundant in cuticular wax and root suberin biosynthesis, but differentially controlled by osmotic stress. *The Plant Journal* **60**: 462–475.

Lee SB, Suh MC. 2015. Advances in the understanding of cuticular waxes in *Arabidopsis thaliana* and crop species. *Plant Cell Reports* **34**: 557–572.

Li C, Haslam TM, Krüger A, Schneider LM, Mishina K, Samuels L, Yang H, Kunst L, Schaffrath U, Nawrath C et al. 2018. The β-ketoacyl-CoA synthase HvKCS1, encoded by Cer-zh, plays a key role in synthesis of barley leaf wax and germination of barley powdery mildew. *Plant and Cell Physiology* **59**: 806–822.

Li H, Guo Y, Cui Q, Zhang Z, Yan X, Ahammed GJ, Yang X, Yang J, Wei C, Zhang X. 2020. Alkanes (C29 and C31)-mediated intracuticular wax accumulation contributes to melatonin- and ABA-induced drought tolerance in watermelon. *Journal of Plant Growth Regulation* **39**: 1441–1450.

Liu L, Jose SB, Campoli C, Bayer MM, Sánchez-Diaz MA, McAllister T, Zhou Y, Eskan M, Milne L, Schreiber M *et al.* **2022.** Conserved signalling components coordinate epidermal patterning and cuticle deposition in barley. *Nature Communications* 13: 6050.

Long LM, Patel HP, Cory WC, Stapleton AE. 2003. The maize epicuticular wax layer provides UV protection. *Functional Plant Biology* 30: 75–81.

Lundqvist U. 2014. Scandinavian mutation research in barley – a historical review. *Hereditas* 151: 123–131.

Lundqvist U, Lundqvist A. 1988. Mutagen specificity in barley for 1580 *eceriferum* mutants localized to 79 loci. *Hereditas* 108: 1–12.

Magwene PM, Willis JH, Kelly JK. 2011. The statistics of bulk segregant analysis using next generation sequencing. *PLoS Computational Biology* 7: e1002255.

Mansour E, Moustafa ESA, Qabil N, Abdelsalam A, Wafa HA, Kenawy AE, Casas AM, Igartua E. 2018. Assessing different barley growth habits under Egyptian conditions for enhancing resilience to climate change. *Field Crops Research* 224: 67–75.

Mascher M, Gundlach H, Himmelbach A, Beier S, Twardziok SO, Wicker T, Radchuk V, Dockter C, Hedley PE, Russell J *et al.* **2017.** A chromosome conformation capture ordered sequence of the barley genome. *Nature* 544: 427–433.

McAllister T, Campoli C, Eskan M, Liu L, McKim SM. 2022. A gene encoding a SHINE1/WAX INDUCER1 transcription factor controls cuticular wax in barley. *Agronomy* 12: 1088.

McCartney AW, Dyer JM, Dhanoa PK, Kim PK, Andrews DW, McNew JA, Mullen RT. 2004. Membrane-bound fatty acid desaturases are inserted co-translationally into the ER and contain different ER retrieval motifs at their carboxy termini. *The Plant Journal* 37: 156–173.

Millar AA, Kunst L. 1997. Very-long-chain fatty acid biosynthesis is controlled through the expression and specificity of the condensing enzyme. *The Plant Journal* 12: 121–131.

Milne L, Bayer M, Rapazote-Flores P, Mayer C-D, Waugh R, Simpson CG. 2021. EORNA, a barley gene and transcript abundance database. *Scientific Data* 8: 90.

Nawrath C. 2006. Unraveling the complex network of cuticular structure and function. *Current Opinion in Plant Biology* 9: 281–287.

Nødskov Giese B. 1975. Effects of light and temperature on the composition of epicuticular wax of barley leaves. *Phytochemistry* 14: 921–929.

Park J, Bae S, Kim J-S. 2015. Cas-Designer: a web-based tool for choice of CRISPR-Cas9 target sites. *Bioinformatics* 31: 4014–4016.

Patwari P, Salewski V, Gutbrod K, Kreszies T, Dresen-Scholz B, Peisker H, Steiner U, Meyer AJ, Schreiber L, Dörmann P. 2019. Surface wax esters contribute to drought tolerance in Arabidopsis. *The Plant Journal* 98: 727–744.

Rentsch D, Laloi M, Rouhara I, Schmelzer E, Delrot S, Frommer WB. 1995. NTR1 encodes a high affinity oligopeptide transporter in *Arabidopsis*. *FEBS Letters* 370: 264–268.

Richardson A, Boscari A, Schreiber L, Kerstiens G, Jarvis M, Herzyk P, Fricke W. 2007. Cloning and expression analysis of candidate genes involved in wax deposition along the growing barley (*Hordeum vulgare*) leaf. *Planta* 226: 1459–1473.

Riederer M, Schreiber L. 2001. Protecting against water loss: analysis of the barrier properties of plant cuticles. *Journal of Experimental Botany* 52: 2023–2032.

Rostás M, Ruf D, Zabka V, Hildebrandt U. 2008. Plant surface wax affects parasitoid's response to host footprints. *Die Naturwissenschaften* 95: 997–1002.

Rowland O, Zheng H, Hepworth SR, Lam P, Jetter R, Kunst L. 2006. CER4 encodes an alcohol-forming fatty acyl-coenzyme A reductase involved in cuticular wax production in Arabidopsis. *Plant Physiology* 142: 866–877.

Sadler C, Schroll B, Zeisler V, Waßmann F, Franke R, Schreiber L. 2016. Wax and cutin mutants of *Arabidopsis*: quantitative characterization of the cuticular transport barrier in relation to chemical composition. *Biochimica et Biophysica Acta (BBA) - Bioenergetics* 1861: 1336–1344.

Schneider LM, Adamski NM, Christensen CE, Stuart DB, Vautrin S, Hansson M, Uauy C, von Wettstein-Knowles P. 2016. The *Cer-cqu* gene cluster determines three key players in a β-diketone synthase polyketide pathway synthesizing aliphatics in epicuticular waxes. *Journal of Experimental Botany* 67: 2715–2730.

Suh MC, Samuels AL, Jetter R, Kunst L, Pollard M, Ohlrogge J, Beisson F. 2005. Cuticular lipid composition, surface structure, and gene expression in Arabidopsis stem epidermis. *Plant Physiology* 139: 1649–1665.

Takagi H, Abe A, Yoshida K, Kosugi S, Natsume S, Mitsuoka C, Uemura A, Utsushi H, Tamiru M, Takuno S *et al.* **2013.** QTL-seq: rapid mapping of quantitative trait loci in rice by whole genome resequencing of DNA from two bulked populations. *The Plant Journal* 74: 174–183.

Tong T, Fang Y-X, Zhang Z, Zheng J, Zhang X, Li J, Niu C, Xue D, Zhang X. 2021. Genome-wide identification and expression pattern analysis of the KCS gene family in barley. *Plant Growth Regulation* 93: 89–103.

Untergasser A, Cutcutache I, Koressaar T, Ye J, Faircloth BC, Remm M, Rozen SG. 2012. Primer3 – new capabilities and interfaces. *Nucleic Acids Research* 40: e115.

Voinnet O, Lederer C, Baulcombe DC. 2000. A viral movement protein prevents spread of the gene silencing signal in *Nicotiana benthamiana*. *Cell* 103: 157–167.

Voisin D, Nawrath C, Kurdyukov S, Franke RB, Reina-Pinto JJ, Efremova N, Will I, Schreiber L, Yephremov A. 2009. Dissection of the complex phenotype in cuticular mutants of Arabidopsis reveals a role of SERRATE as a mediator. *PLoS Genetics* 5: e1000703.

Wang M, Wang Y, Wu H, Xu J, Li T, Hegebarth D, Jetter R, Chen L, Wang Z. 2016. Three TaFAR genes function in the biosynthesis of primary alcohols and the response to abiotic stresses in *Triticum aestivum*. *Scientific Reports* 6: 25008.

Wang W, Zhang Y, Xu C, Ren J, Liu X, Black K, Gai X, Wang Q, Ren H. 2015. Cucumber ECERIFERUM1 (CsCER1), which influences the cuticle properties and drought tolerance of cucumber, plays a key role in VLC alkanes biosynthesis. *Plant Molecular Biology* 87: 219–233.

Wang Y, Sun Y, You Q, Luo W, Wang C, Zhao S, Chai G, Li T, Shi X, Li C *et al.* **2018.** Three fatty acyl-coenzyme A reductases, BdFAR1, BdFAR2 and BdFAR3, are involved in cuticular wax primary alcohol biosynthesis in *Brachypodium distachyon*. *Plant and Cell Physiology* 59: 527–543.

Wang Y, Wang M, Sun Y, Hegebarth D, Li T, Jetter R, Wang Z. 2015a. Molecular characterization of TaFAR1 involved in primary alcohol biosynthesis of cuticular wax in hexaploid wheat. *Plant and Cell Physiology* 56: 1944–1961.

Wang Y, Wang M, Sun Y, Wang Y, Li T, Chai G, Jiang W, Shan L, Li C, Xiao E *et al.* **2015b.** FAR5, a fatty acyl-coenzyme A reductase, is involved in primary alcohol biosynthesis of the leaf blade cuticular wax in wheat (*Triticum aestivum* L.). *Journal of Experimental Botany* 66: 1165–1178.

Weidenbach D, Jansen M, Bodewein T, Nagel KA, Schaffrath U. 2015. Shoot and root phenotyping of the barley mutant kcs6 (3-ketoacyl-CoA synthase6) depleted in epicuticular waxes under water limitation. *Plant Signaling & Behavior* 10: 1–3.

Weyers JDB, Travis AJ. 1981. Selection and preparation of leaf epidermis for experiments on stomatal physiology. *Journal of Experimental Botany* 32: 837–850.

Wu H, Le Liu CY, Liu T, Jiang Q, Wei Z, Li C, Wang Z. 2022. Tomato SlCER1-1 catalyzes the synthesis of wax alkanes which increases the drought tolerance and fruit storability. *Horticulture Research* 9: uhac004.

Wu P, Xie J, Hu J, Qiu D, Liu Z, Li J, Li M, Zhang H, Yang L, Liu H *et al.* **2018.** Development of molecular markers linked to powdery mildew resistance gene Pm4b by combining SNP discovery from transcriptome sequencing data with bulked segregant analysis (BSR-Seq) in wheat. *Frontiers in Plant Science* 9: 95.

Zeisler V, Schreiber L. 2016. Epicuticular wax on cherry laurel (*Prunus laurocerasus*) leaves does not constitute the cuticular transpiration barrier. *Planta* 243: 65–81.

Zeisler-Diehl V, Müller Y, Schreiber L. 2018. Epicuticular wax on leaf cuticles does not establish the transpiration barrier, which is essentially formed by intracuticular wax. *Journal of Plant Physiology* 227: 66–74.

Zhang S, Wu S, Niu C, Liu D, Yan T, Tian Y, Liu S, Xie K, Li Z, Wang Y *et al.* **2021.** *ZmMs25* encoding a plastid-localized fatty acyl reductase is critical for anther and pollen development in maize. *Journal of Experimental Botany* 72: 4298–4318.

Zhang X, Henriques R, Lin S-S, Niu Q-W, Chua N-H. 2006. Agrobacterium-mediated transformation of *Arabidopsis thaliana* using the floral dip method. *Nature Protocols* 1: 641–646.

Supporting Information

Additional Supporting Information may be found online in the Supporting Information section at the end of the article.

Fig. S1 Cuticular wax composition in leaves of Bowman and the *cer-za.227* and *cer-ye.267* mutants.

Fig. S2 Wax ester composition in leaves of the Bowman and the *cer-za.227* mutant.

Fig. S3 Identification of the *CER-ZA* locus using bulked segregant RNA sequencing (BSR-Seq).

Fig. S4 Phylogenetic tree of amino acid sequences with similarity to acyl-CoA reductases (FAR) from different plant species.

Fig. S5 Identification of the *CER-YE* locus using bulked segregant RNA sequencing (BSR-Seq).

Fig. S6 Residual permeance P (m s^{-1}) giving the cuticular transpiration of five detached leaves plotted against the relative water deficit (RWD).

Methods S1 Bulked segregant analysis RNA sequencing (BSR-Seq) and bioinformatic and phylogenetic analyses.

Table S1 Cultivars and mutant lines of barley (*Hordeum vulgare*) used in this study.

Table S2 Oligonucleotides used in this study.

Table S3 Expression patterns derived from BSR-Seq experiments in Bowman and *cer-za.227*.

Table S4 Paralogous sequences of *HORVU5Hr1G089230* in barley.

Table S5 Single-nucleotide polymorphisms (SNPs) in *HORVU5Hr1G089230* in the cultivars Morex and Foma and in the *cer-za* mutant alleles.

Table S6 Expression patterns derived from BSR-Seq experiments in Bowman and *cer-ye.267*.

Please note: Wiley is not responsible for the content or functionality of any Supporting Information supplied by the authors. Any queries (other than missing material) should be directed to the *New Phytologist* Central Office.